International Journal of Thermophysics, Vol. 27, No. 2, March 2006 (© 2006)
DOI: 10.1007/s10765-005-0011-4

Density and Thermal Expansion of Liquid Ag–Cu and Ag–Au Alloys

J. Brillo,[1,2] I. Egry,[1] and I. Ho[1]

Received May 9, 2005

The densities of liquid Cu–Ag and Ag–Au alloys were measured using the technique of electromagnetic levitation. This technique involves producing shadow images of the sample from which the volume is calculated by an image processing algorithm. The density and thermal expansion of several alloys and the pure elements copper, gold, and silver are measured at temperatures above their melting points. In addition, they were investigated as a function of either the copper or gold concentration. It was found from data analysis that the densities can be derived from a linear combination of the molar volumes of the elements and that thermodynamic excess quantities are negligibly small.

KEY WORDS: Cu–Au and Ag–Au alloys; density; electromagnetic levitation; thermal expansion; thermophysical properties.

1. INTRODUCTION

Thermophysical properties of liquid metals, such as density and thermal expansion, are important for both technical applications and physical understanding. The aim of this work is to study systems that have comparatively high densities, such as the binary Cu–Ag and Ag–Au alloys. Both systems serve as test systems to explore the limits of electromagnetic levitation for samples of high densities.

Obviously, the force required to levitate a sample is proportional to its mass. Therefore, problems with the equilibrium position and visibility of these samples were to be expected. In addition, the low emissivity and

[1] Deutsches Zentrum für Luft- und Raumfahrt, Institut für Raumsimulation, D-51170 Köln, Germany.
[2] To whom correspondence should be addressed. E-mail: Juergen.Brillo@dlr.de

relatively low liquidus temperature of these alloys require an effective gas-cooling system. Together with an earlier publication on Au–Cu [1], this paper gives a complete account on the densities of liquid binary alloys of precious metals.

Up to now, there have not been many density data published for these systems. In 1929, Krause and Sauerwald [2] published densities of liquid Cu–Ag that were determined using a buoyancy method. Density data of liquid Ag–Au alloys, measured with the same technique, were reported by Gebhardt and Dorner [3] in 1951. In this method, the density of the sample is determined from the buoyancy force that is produced from the difference in the specific weight between the sample and the surrounding liquid salt. The measurement of the thermal expansion is difficult to achieve with this method because it requires a knowledge of the thermal expansion of the liquid salt. Techniques of higher experimental accuracy have meanwhile become available, and a reassesment of the existing density data seems to be appropriate. It is therefore another goal of this work to provide an update of the existing set of density data for Cu–Ag and Ag–Au.

The density, $\rho(T)$, of a liquid metal can be considered to be a linear function of temperature, T, within a limited temperature interval including the melting point:

$$\rho(T) = \rho_{\mathrm{L}} + \rho_{\mathrm{T}}(T - T_{\mathrm{L}}) \tag{1}$$

In this equation, ρ_{L} is the density at the liquidus temperature, T_{L}, and ρ_{T} is the constant temperature gradient $\partial\rho/\partial T$.

For a solution of N components A_i $(i = 1, \ldots, N)$ with atomic concentrations c_i and respective molar masses M_i, the molar volume of the solution, V, is generally represented by [4]

$$V = \sum_{i=1}^{N} c_i \frac{M_i}{\rho_i} + V^E \tag{2}$$

where the ρ_i are the densities of the pure substances A_i at the same temperature T. V^{E} is the excess volume. For $V^{\mathrm{E}} = 0$, Eq. (2) reduces to a simple linear combination of the molar volumes, which is often referred to as Vegard's law [5].

If in Eq. (2) the excess volume, V^{E}, is assumed independent of temperature, the following expression can be derived for ρ_{T}:

$$\rho_{\mathrm{T}} = \frac{\partial\rho(T)}{\partial T} = \frac{\left[\sum_i c_i M_i\right] \times \left[\sum_i c_i \frac{M_i \rho_{\mathrm{T,i}}}{\rho_i^2}\right]}{V^2} \tag{3}$$

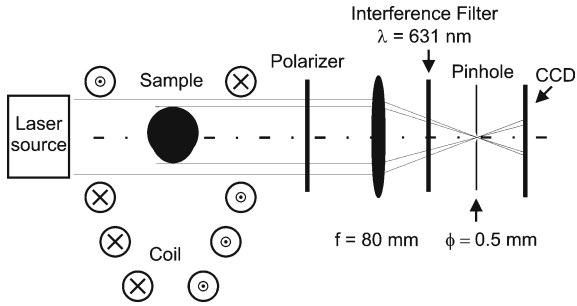

Fig. 1. Schematic diagram of the optical setup.

In this expression, $\rho_{T,i}$ is the thermal coefficient of the density of the pure component A_i.

2. EXPERIMENTAL

All experiments presented in this work were carried out in an electromagnetic levitation chamber that is described in detail in Refs. 6 and 7. The experimental setup is shown schematically in Fig. 1. The sample is processed under a protecting atmosphere of He/8vol%-H_2 in a levitation coil. Positioning and melting are achieved through inductive interactions between the alternating, inhomogeneous electromagnetic field and the electrically conducting sample.

Temperature control is maintained by carefully cooling the sample in a laminar flow of the He/H_2 gas mixture, which is admitted from below via a ceramic tube. The temperature, T, is measured using an infrared pyrometer aimed at the top of the sample. For each sample, it is necessary to recalibrate the temperature with respect to the liquidus temperature, T_L, which is taken from Ref. 8. If T_P is the output signal from the pyrometer, then the real temperature T is obtained using the following approximation derived from Wien's law:

$$\frac{1}{T} - \frac{1}{T_P} = \frac{1}{T_L} - \frac{1}{T_{L,P}} \tag{4}$$

In Eq. (4), $T_{L,P}$ is the pyrometer signal at the liquidus temperature, T_L. As shown in Fig. 2, $T_{L,P}$ is identified by a sudden increase in the slope of T_P that occurs when the melting process is completed and the sample temperature, T, exceeds T_L. Equation (4) is valid only if the sample emissivity at the operating wavelength of the pyrometer $\varepsilon_\lambda(T)$ remains

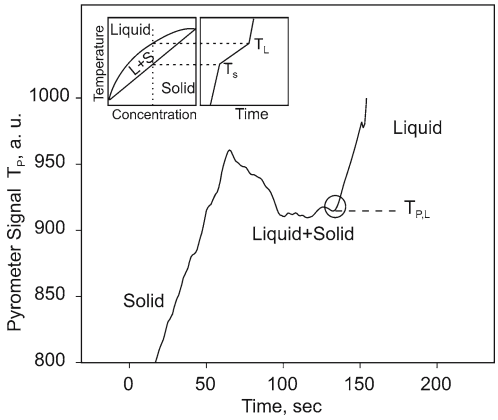

Fig. 2. Typical pyrometer output, T_P, when the sample melts. The value $T_{P,L}$ is used to calibrate the pyrometer signal with respect to the known liquidus temperature T_L. $T_{P,L}$ is identified by a sudden change in the slope of the curve as illustrated by the insert.

constant over the experimentally scanned range of temperature. This is a good approximation for most metals; see Ref. 9.

To measure the volume, shadowgraphs are taken of the levitated sample. A polarized HeNe laser beam, equipped with a spatial filter and a beam expander, is used to illuminate the sample from behind. The shadow image is captured by means of a digital CCD camera. It is analyzed by an edge detection algorithm that locates the edge curve $R(\varphi)$ where R is the radius and φ is the azimuthal angle in polar coordinates. In order to eliminate the influence of the droplet's oscillations, the edge curve is averaged over 800 frames. The averaged edge curve is then fitted by Legendre polynomials of order $\leqslant 6$;

$$\langle R(\varphi)\rangle = \sum_{i=0}^{6} a_i P_i(\cos(\varphi)) \tag{5}$$

with P_i being the ith Legendre polynomial. The equilibrium shape of the sample is to a good approximation symmetric with respect to the vertical axis as shown by an analysis of top view images [6]. Hence, its volume is calculated using the following integral:

$$V_P = \frac{2}{3}\pi \int_0^{\pi} \langle R(\varphi)\rangle^3 \sin(\varphi) d\varphi \tag{6}$$

V_p is the volume in pixel units. It is related to the real volume V by $V = q \cdot V_P$ where q is a proportionality factor that is determined in a procedure described in Ref. 6.

When M is the mass of the sample, the density, ρ, is calculated from $\rho = MV^{-1}$. In order to check whether the mass remained constant over the duration of the experiment each sample is weighed immediately before and after the measurement. In the case where the mass loss was more than $\approx$ 0.3%, the measurement was disregarded.

In order to estimate uncertainties of our data, contributions from the following sources of error were considered: mass loss during the experiment, Δm, error in calibration, Δq, scatter, ΔT, of the temperature signal, and a relative scatter of the measured uncalibrated volumes $\Delta V_P(T)$ which is obtained from the mean deviation of V_P from the linear fit of V_P to the temperature T. All other influences were neglected. The uncertainties of ρ and ρ_T reported in this work were estimated from these contributions for each measurement individually using the following equations:

$$\frac{\Delta\rho^2}{\rho^2} = \frac{\Delta m^2}{m^2} + \frac{\Delta q^2}{q^2} + \frac{\Delta V_P^2}{V_P^2} + \left(\frac{\partial V_P}{\partial T}\right)^2 \frac{\Delta T^2}{V_P^2} \tag{7}$$

$$\frac{\Delta\rho_T^2}{\rho^2} = V_P^{-2}\left(\frac{\partial V_P}{\partial T}\right)^2 \left\{\frac{\Delta m^2}{m^2} + \frac{\Delta q^2}{q^2} + 4\frac{\Delta V_P^2}{V_P^2}\right\} \tag{8}$$

In principle there is also an uncertainty, ΔT_L, of the reported liquidus temperatures used in Eq. (4) in order to calibrate the pyrometer. Taking it into account, however, would require a general review and discussion of the published phase diagrams. Moreover, the phase diagrams and liquidus temperatures of Ag–Cu and Ag–Au reported in Ref. 8 are generally accepted and it is therefore justified to neglect ΔT_L in the present study.

3. RESULTS AND DISCUSSION

All samples could easily be levitated and were fully visible from the side. As long as the temperature was kept lower than approximately $T_L + 250\,K$, mass loss due to the evaporation of silver was low.

The densities of the pure elements, $\rho(T)$, are listed in Table I and shown in Fig. 3. It is obvious from Fig. 3 that for each element the density can be decribed as a linear function of the temperature. Hence, Eq. (1) can be fitted to the data. The corresponding fit parameters, ρ_L and ρ_T are summarized in Table II together with their uncertainties calculated from Eqs. (7) and (8), respectively.

Table I. Experimental Density Data for Copper, Silver, and Gold

Copper		Silver		Gold	
T (°C)	$\rho(T)$ (g·cm^{-3})	T (°C)	$\rho(T)$ (g·cm^{-3})	T (°C)	$\rho(T)$ (g·cm^{-3})
1127	7.89	1107	9.04	1506	16.87
1217	7.78	1067	9.08	1467	16.93
1291	7.73	1025	9.09	1387	17.03
1379	7.67	1009	9.11	1361	17.06
1438	7.66	985	9.14	1310	17.08
1525	7.56	1038	9.1	1423	17.05
		977	9.14	1436	16.97
				1282	17.17
				1245	17.20
				1207	17.28
				1184	17.26
				1154	17.26
				1113	17.35
				1085	17.34

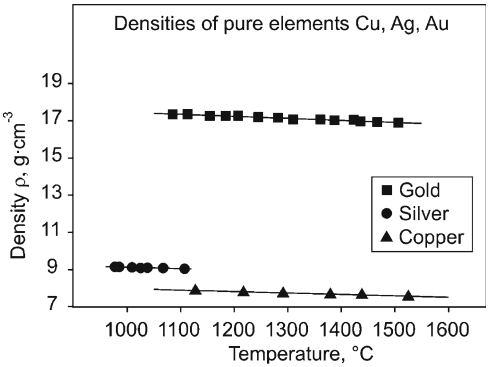

Fig. 3. Density data of the pure elements copper, silver, and gold vs. temperature.

The uncertainties of ρ_L are less than 1%. The thermal coefficients of copper, $\rho_T = -7.7 \times 10^{-4}\,g \cdot cm^{-3} \cdot K^{-1}$, and silver, $\rho_T = -7.4 \times 10^{-4}\,g \cdot cm^{-3} \cdot K^{-1}$, are similar but that of gold is slightly lower, $\rho_T = -11.0 \times 10^{-4}\,g \cdot cm^{-3} \cdot K^{-1}$. The relative uncertainty $\Delta\rho_T/\rho_T$ is approximatly 10%.

Generally, there is good agreement with literature data [2, 3, 10–15]. However, in the case of copper and gold, the values for ρ_T given

Table II. Parameters ρ_L and ρ_T of Pure Copper, Silver, and Gold Compared with Literature Data

System	T_L (°C)	ρ_L ($g \cdot cm^{-3}$)	ρ_T ($10^{-4} g \cdot cm^{-3} \cdot K^{-1}$)	Reference
Cu	1084	7.90 ± 0.1	-7.65 ± 0.5	This work
		7.98	−15	[2]
		7.92	−8.4	[10]
		8.03	−7.9	[11]
		8.09	−9.4	[12]
Ag	962	9.15 ± 0.12	-7.4 ± 0.8	This work
		9.24	−6.5	[2]
		9.28	−9.0	[3]
		9.32	−9.78	[13]
		9.31	−10.1	[14]
Au	1064	17.4 ± 0.1	-11.0 ± 0.6	This work
		17.3	−16.1	[3]
		17.2	−12.7	[15]

Table III. Compositions and Liquidus Temperatures of the Investigated Alloys

Cu–Ag		Ag–Au	
c_{Cu} (at%)	T_L (°C)	c_{Au} (at%)	T_L (°C)
20	862	0.25	1003
40	780	0.5	1033
60	859	0.75	1053
80	952		

by Krause and Sauerwald [2] and Gebhardt and Dorner [3] seem to be significantly lower. This might be explained by the previously described inaccuracy in the correction of the thermal expansion of the salt melt that has been used in the applied buoyancy method.

The binary Cu–Ag and Ag–Au alloys were produced by melting together the required amounts of the pure substances in an arc furnace. The compositions and liquidus temperatures of the investigated samples are shown in Table III for the two systems, Cu–Ag and Ag–Au.

The results of the density measurements are shown in Tables IV and V. They are plotted vs. temperature, T, for Cu–Ag in Fig. 4 and for Ag–Au in Fig. 5. Like the pure elements, the densities of the alloys can be described by linear functions of the temperature T. Obviously, there is a steady increase of ρ with an increase of the concentration of the component with the higher molar mass, i.e., silver in Cu–Ag and gold in Ag–Au.

Table IV. Experimental Density Data for the Investigated Ag–Cu Samples

Ag– 20 at%Cu		Ag– 40 at%Cu		Ag– 60 at%Cu		Ag– 80 at%Cu	
T (°C)	ρ(T) ($g \cdot cm^{-3}$)	T (°C)	ρ(T) ($g \cdot cm^{-3}$)	T (°C)	ρ(T) ($g \cdot cm^{-3}$)	T (°C)	ρ(T) ($g \cdot cm^{-3}$)
900	9.05	915	8.83	907	8.59	997	8.32
947	9.05	952	8.82	908	8.61	1017	8.29
998	8.97	998	8.77	927	8.60	1029	8.28
1004	8.97	1045	8.76	936	8.60	1031	8.27
1005	9.0	1045	8.73	941	8.60	1054	8.29
1006	8.96	1089	8.71	942	8.59	1057	8.22
1042	8.95	1123	8.71	963	8.57	1064	8.22
1053	8.97	1123	8.70	977	8.60	1069	8.22
1088	8.94	1130	8.68	995	8.57	1083	8.18
1095	8.91	1148	8.70	998	8.57	1098	8.22
		1164	8.68	1013	8.52	1110	8.18
		1180	8.64	1085	8.50		
		1208	8.63				

Table V. Experimental Density Data for the Investigated Ag–Au Samples

Ag– 25 at%Au		Ag– 50 at%Au		Ag– 75 at%Au	
T (°C)	ρ(T) ($g \cdot cm^{-3}$)	T (°C)	ρ(T) ($g \cdot cm^{-3}$)	T (°C)	ρ(T) ($g \cdot cm^{-3}$)
1043	11.33	1062	13.33	1092	15.62
1061	11.33	1070	13.24	1123	15.56
1069	11.21	1074	13.27	1153	15.56
1074	11.24	1146	13.24	1154	15.63
1084	11.29	1179	13.20	1163	15.31
1085	11.26	1180	13.17	1171	15.28
1111	11.22	1201	13.17	1194	15.29
1117	11.24	1237	13.22	1197	15.18
1121	11.21	1268	13.15	1225	15.46
1125	11.19	1305	13.13	1260	15.45
1128	11.24			1264	15.40
1164	11.19				
1174	11.27				
1209	11.19				
1245	11.14				

In Fig. 4, the scatter of the data is sligthly increased for the Ag – 80 at%Cu sample because it temporarily became unstable in the coil and then was not fully visible from the side. In Fig. 5, the densities of the Ag – 75 at%Au sample are shifted towards lower values for temperatures between

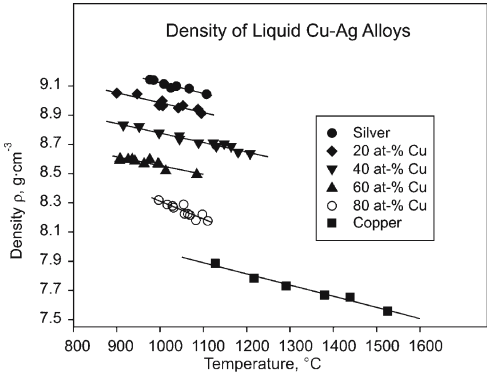

Fig. 4. Density data of liquid Cu–Ag alloys vs. temperature.

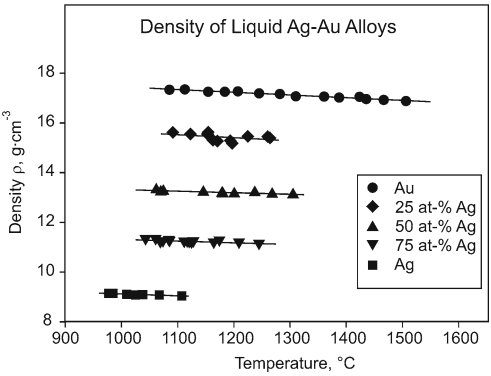

Fig. 5. Density data of liquid Ag–Au alloys vs. temperature.

1160 and 1200°C. In this temperature range, the sample performs strong rotations which lead to a violation of the axisymmetry and hence Eq. (6) is not valid anymore. A large error of ρ_T will therefore result for both of the two samples.

In order to study the concentration dependence of the densities, Eq. (1) was fitted to the data. From the fit parameters ρ_L and ρ_T (Table VI), the densities were calculated at $T = 1000°C$ and plotted as a function of concentration in Figs. 6 and 7 for the two binary systems. These values are in good agreement with the literature values of Krause and Sauerwald [2] and Gebhardt and Dorner [3], which are shown in Figs. 6 and 7 as well.

Table VI. Parameters ρ_L and ρ_T of the Investigated Alloy Samples and Extrapolated Density Values at $T = 1000°C$

System	T_L (°C)	$\rho_L(g \cdot cm^{-3})$	ρ_T $(10^{-4} g \cdot cm^{-3} \cdot K^{-1})$	$\rho(T = 1000°C)$ $(g \cdot cm^{-3})$
Ag – 20 at%Cu	862	9.0 ± 0.2	-6 ± 1.0	8.9
Ag – 40 at%Cu	780	8.9 ± 0.1	-7 ± 0.5	8.8
Ag – 60 at%Cu	859	8.6 ± 0.1	-6 ± 1.2	8.5
Ag – 80 at%Cu	952	8.4 ± 0.3	-12 ± 4.0	8.0
Ag – 25 at%Au	1003	11.2 ± 0.2	-7 ± 2	11.2
Ag – 50 at%Au	1033	13.3 ± 0.3	-6 ± 1	13.3
Ag – 75 at%Au	1053	15.6 ± 1.3	-12 ± 9	15.7

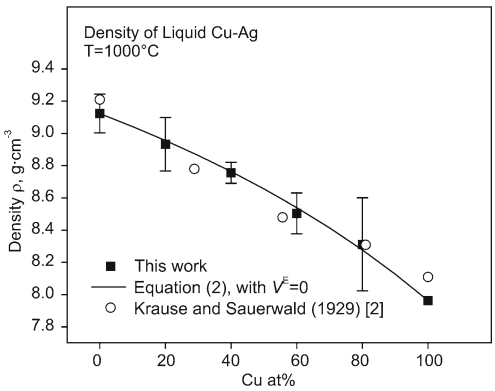

Fig. 6. Density of liquid Cu–Ag at $T = 1000°C$ as a function of copper concentration in comparison to data taken from Ref. 2.

In the case of both binary alloy systems, the density can be described as a function of concentration by Eq. (2) with the excess volume being set to zero, i.e., $V^E = 0$. The deviation of the experimental data from this calculation appears to be even less than that of the previously published data. It is also less than the uncertainty of the data, obtained from Eq. (7), which is $\pm 1\%$. The fact that no excess volume is needed in order to describe the data is not surprising, since this behavior has also been observed in another similar case for the Cu–Au system [1]. For the liquid state, it can therefore be concluded that $V^E = 0$ for the three possible binary alloys of the group 1b elements. This, however, is not true for the solid state, where Ag–Au has a negative and Cu–Au has a positive excess volume [16].

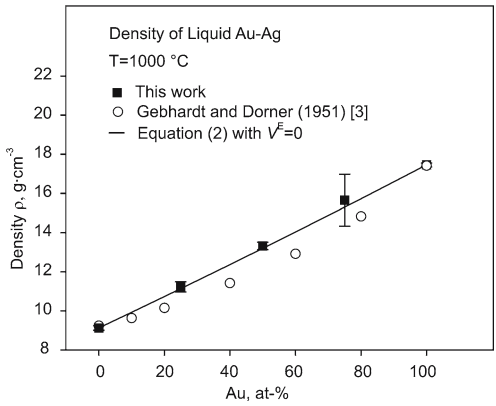

Fig. 7. Density of liquid Ag–Au at $T = 1000°C$ as a function of gold concentration in comparison to data taken from Ref. 3.

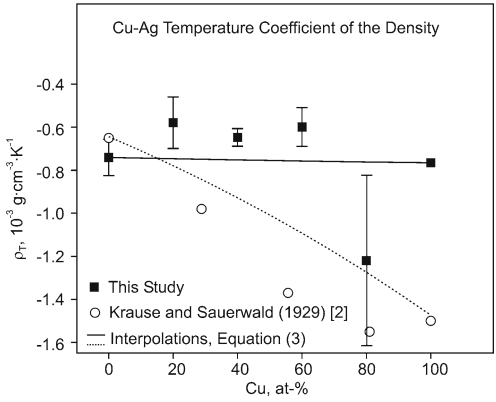

Fig. 8. Thermal density coefficient, ρ_T, of Cu–Ag vs. copper concentration in comparison to data taken from Ref. 2.

Knowing $V^E = 0$, it is possible to use Eq. (3) in order to predict the thermal coefficients of the density, ρ_T. This is demonstrated in Fig. 8 for Cu–Ag and in Fig. 9 for Ag–Au. The agreement between the calculated and measured values is reasonable, although the uncertainties for determing ρ_T are generally larger than for the determination of ρ_L. In particular, the uncertainty of ρ_T is increased for Ag – 80 at%Au due to its restricted visibility from the side and for Ag – 75 at%Au due to the strong

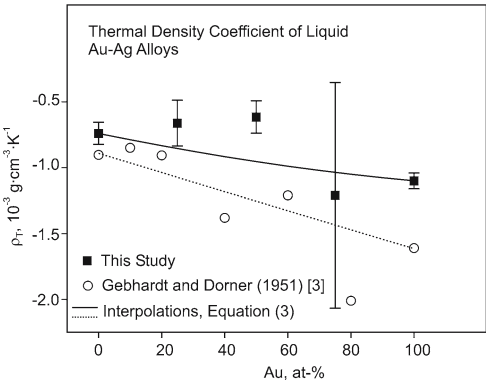

Fig. 9. Thermal density coefficient, ρ_T, of Ag–Au vs. gold concentration in comparison to data taken from Ref. 3.

rotations that the sample temporarily performed; see above and Figs. 4 and 5.

The values of ρ_T given by Krause and Sauerwald [2] and Gebhardt and Dorner [3] are shown in Figs. 8 and 9 as well. Their data can also be described by Eq. (3), provided that their own values of ρ_T for copper and gold are used (dotted lines). However, there seem to be systematic deviations from our values which increase with the concentrations of copper in Fig. 8 and gold in Fig. 9. The reason for these deviations is probably the same as already discussed above for the case of the pure elements copper and gold – namely the thermal expansion of the salt melt. Hence, we are inclined to believe that our results for ρ_T are more accurate.

4. CONCLUSION

The investigated Cu–Ag and Ag–Au samples were easily levitated electromagnetically. For each sample the density can be described as a linear function of temperature. The measured densities increase with increasing silver content in Cu–Ag and gold content in Ag–Au. It was found that the densities and thermal expansions can be described by a linear combination of molar volumes and that the excess volume is negligibly small.

REFERENCES

1. J. Brillo, I. Egry, H. S. Giffard, and A. Patti, *Int. J. Thermophys.* **25**:1535 (2004).
2. W. Krause and F. Sauerwald, *Z. Anorg. Allg. Chem.* **181**:347 (1929).

3. E. Gebhardt and S. Dorner, *Z. Metallkd.* **42**:353 (1951).
4. C. Lüdecke and D. Lüdecke, *Thermodynamik* (Springer, Heidelberg, 2000), p. 506.
5. L. Vegard, *Z. Phys*. **5**:17 (1921).
6. J. Brillo and I. Egry, *Int. J. Thermophys*. **24**:1155 (2003).
7. J. Brillo and I. Egry, *Z. Metallkd*. **95**:691 (2004).
8. T. B. Massalski, *Binary Alloy Phase Diagrams* (American Society for Metals, Materials Park, Ohio, 1986).
9. S. Krishnan, G. P. Hansen, R. H. Hauge, and J. L. Margrave, *High Temp. Sci*. **29**:17 (1990).
10. E. Gorges, *Bestimmung der Dichte und Oberflächenspannung von levitierten flüssigen Metallegiergungen am Beispiel des Systems Kupfer-Nickel* (Ph. D. Thesis, Rheinisch-Westfälische-Technische Hochschule, Aachen, Germany, 1996).
11. A. Saito and S. Watanabe, *Nipp. Kinz. Gakk*. **35**:554 (1971).
12. A. E. El-Mehairy and R. G. Ward, *Trans. Met. Soc. AIME* **227**:1226 (1963).
13. L. Martin-Garin, M. Gomez, P. Bedon, and P. Desre, *J. Less-Common Metals* **41**:65 (1975).
14. Y. Matuyama, *Sci. Rep. Tohoku Imp. Univ.* **20**:8 (1937).
15. G. P. Khilya, Yu. N. Ivachshenko, and V. N. Eremenko, *Izv. Akad. Nauk SSSR, Met*. **6**:87 (1975).
16. W. B. Pearson, *Handbook of Lattice Spacing and Structure of Metals* (Pergamon, New York, 1967).